see commentary on page 363

# Transglutaminase inhibition ameliorates experimental diabetic nephropathy

Linghong Huang[1], John L. Haylor[1], Zoe Hau[1], Richard A. Jones[2,*], Melissa E. Vickers[1], Bart Wagner[3], Martin Griffin[4], Robert E. Saint[2], Ian G.C. Coutts[2], A. Meguid El Nahas[1] and Timothy S. Johnson[1]

*[1]Academic Nephrology Unit, Sheffield Kidney Institute, School of Medicine and Biomedical Sciences, University of Sheffield, Sheffield, UK; [2]Biomedical Sciences, School of Science and Technology, Nottingham Trent University, Nottingham, UK; [3]Department of Histology, Northern General Hospital, Sheffied, UK and [4]School of Health and Life Sciences, Aston University, Birmingham, UK*

**Diabetic nephropathy is characterized by excessive extracellular matrix accumulation resulting in renal scarring and end-stage renal disease. Previous studies have suggested that transglutaminase type 2, by formation of its protein crosslink product ε-(γ-glutamyl)lysine, alters extracellular matrix homeostasis, causing basement membrane thickening and expansion of the mesangium and interstitium. To determine whether transglutaminase inhibition can slow the progression of chronic experimental diabetic nephropathy over an extended treatment period, the inhibitor NTU281 was given to uninephrectomized streptozotocin-induced diabetic rats for up to 8 months. Effective transglutaminase inhibition significantly reversed the increased serum creatinine and albuminuria in the diabetic rats. These improvements were accompanied by a fivefold decrease in glomerulosclerosis and a sixfold reduction in tubulointerstitial scarring. This was associated with reductions in collagen IV accumulation by 4 months, along with reductions in collagens I and III by 8 months. This inhibition also decreased the number of myofibroblasts, suggesting that tissue transglutaminase may play a role in myofibroblast transformation. Our study suggests that transglutaminase inhibition ameliorates the progression of experimental diabetic nephropathy and can be considered for clinical application.**

*Kidney International* (2009) **76,** 383–394; doi:10.1038/ki.2009.230; published online 24 June 2009

KEYWORDS: collagen; crosslink; diabetic nephropathy; extracellular matrix; renal scarring; transglutaminase

**Correspondence:** *Timothy S. Johnson, Academic Nephrology Unit, Sheffield Kidney Institute, Room GU24, School of Medicine and Biomedical Sciences, The University of Sheffield, Royal Hallamshire Hospital, Beech Hill Road, Sheffield S10 2RZ, UK. E-mail: t.johnson@sheffield.ac.uk*

*The study is dedicated to the memory of Dr Richard Jones who died tragically while completing this study.

**Received 14 August 2008; revised 30 April 2009; accepted 5 May 2009; published online 24 June 2009**

Diabetic nephropathy (DN) is the most common cause of end-stage renal disease[1,2] accounting for 50% of cases requiring renal replacement therapy in the United States.[3] This is due to the increasing prevalence of type 2 diabetes and the reduced mortality of DN patients resulting from better management. Diabetic patients now live longer and patients with diabetic end-stage renal disease are now being accepted for treatment in dialysis programs where formerly they might have been excluded.

Clinically, the progression of DN is accompanied by the development of proteinuria and early glomerular hyperfiltration followed by a decline of glomerular filtration rate. Morphologically, it is characterized by excessive renal extracellular matrix (ECM) accumulation in the glomeruli and tubulointerstitial space, causing glomerulosclerosis and tubulointerstitial fibrosis. This ultimately leads to end-stage renal disease.

Transglutaminase type 2 (TG2) is a calcium-dependent enzyme that catalyzes an acyl-transfer reaction (EC 2.3.2.13) between the γ-carboxamide group of peptide-bound glutamine and the ε-amino group of peptide-bound lysine. This leads to the formation of a stable and proteolytic-resistant ε-(γ-glutamyl)lysine dipeptide bond, resulting in intra- or intermolecular crosslinks in protein. A number of extracellular proteins including fibronectin,[4] collagen,[5] fibrinogen,[6] osteopontin,[7] laminin, and nidogen[8] are TG2 substrates. When TG2 is released from the cell, the high extracellular $Ca^{2+}$ and low GTP (which modulates $Ca^{2+}$ activation of the enzyme) activates the enzyme, enabling crosslinking of these ECM proteins at the cell surface and in the surrounding matrix. Crosslinking of collagen by TG2 has been associated with stabilization of the collagen fibril independently of lysyl oxidase,[5] accelerated ECM deposition,[9] reduced proteolytic breakdown of the ECM,[10] and ultimately lower ECM turnover.[11] Thus, TG2 action shifts the ECM deposition–degradation balance toward accumulation[12] and has subsequently been linked to a range of fibrogenic conditions.

A role for TG2 in the pathogenesis of DN has been reported in both the streptozotocin (STZ)-induced model of type 1 diabetes[13] and human diabetic kidney disease,[14] with increased TG2-mediated ε-(γ-glutamyl)lysine crosslink

formation in diabetic kidneys tightly associated with both glomerular and tubulointerstitial ECM expansion. Currently, there remains no viable mechanism for interfering with this ECM buildup. Subsequently, the development of therapeutic approaches directly targeting this process may provide an effective approach to the prevention of DN as well as numerous other fibrotic conditions. The inhibition of TG activity in proximal tubular epithelial cells in culture has already been shown to reduce glucose-induced ECM accumulation,[15] providing strong support for the *in vivo* application of such compounds in the treatment for DN. Therefore, in this study, the TG site-directed irreversible inhibitor *N*-benzyloxycarbonyl-L-phenylalanyl-6-dimethylsulfonium-5-oxo-L-norleucine (NTU281) has been applied by direct intrarenal infusion into the kidneys of rats receiving STZ injection and by uninephrectomy over an 8-month treatment period. NTU281 is a benzyloxycarbonyl phenylalanyl analog containing a dimethylsulfonium group that binds the cysteine residue in the active site of TG to instigate an acetonylation reaction leading to permanent noncompetitive inhibition of the enzyme.[16] Whereas the STZ model is not a direct representative of DN in humans as it lacks the characteristic histological lesions, it is a useful surrogate for the impact of sustained hyperglycemia on changes in ECM turnover in the kidney. Uninephrectomy has been used to accelerate diabetic kidney changes.[17,18] We report that TG inhibition can preserve kidney function, reduce albuminuria, and ameliorate the progression of the histological changes associated with the formation of scar tissue in DN.

## RESULTS

### Verification of drug delivery

To ascertain if intrarenal cannulation was achieving uniform drug delivery throughout the kidney, we prepared a dansyl-labeled version of NTU281. Using a kidney that was cannulated 28 days previously (to allow the fibrous coat around the cannula to develop) and had received phosphate-buffered saline from implant, we infused 50 mM dansyl-labeled NTU281 for 24 h. Cryostat sections viewed under a fluorescent microscope showed a uniform distribution of dansyl-NTU281 in both the longitudinal and the transverse planes in comparison with the contralateral kidney where no fluorescence was visible (Figure 1a). Import of images into multianalyst image analysis software allowed densitometric profile assessment of the fluorescence, which confirmed equal distribution in both planes (Figure 1b).

### Experimental groups

Four experimental groups were used. Normal, uninephrectomy (UNx), UNx + Streptozotocin (STZ) (referred to as diabetic or DM), and UNx + STZ + Transglutaminase inhibitor NTU281 (referred to as diabetic treated).

### General observations

Calculation of osmotic pump delivery rates from residual pump volumes showed a consistent drug delivery throughout the treatment period (Figure 2a). Examination of cannulas at termination indicated that all had remained *in situ* and there was no evidence of cannula leakage.

Compared with normal and UNx animals, both diabetic groups (that is, treated and untreated with NTU281) had higher levels of blood glucose throughout the experimental period (Figure 2c) and within the 10–25 mmol/l target range using a comparable insulin dose (Figure 2b), thus showing an equal metabolic burden in treated and untreated rats.

In hyperglycemic animals by 8 months post-STZ, body weight gain was approximately twofold lower (Figure 2d) than that in normal rats, reaching 355 ± 12.8 and 377 ± 14.3 g in diabetic and NTU281-treated diabetic rats, respectively, compared with 546 ± 22.6 g in normal (Table 1).

Kidney weight following UNx was greater than that in normal, but only significantly at 1 month post-STZ (Table 1). Imposing hyperglycemia caused a marked increase in kidney weight, being more than threefold greater by 8 months; however, TG inhibition reduced increased kidney weight by 42% at this point (Table 1).

Although blood pressure was raised in hyperglycemic animals, there was no significant difference in systolic blood pressure between the four groups throughout the study (not shown).

### Effectiveness of TG inhibition

TG *in situ* activity assays showed a sixfold increase in extracellular TG activity in the untreated diabetic animals by 8 months (Figure 3i). Increased extracellular TG activity was present both in the glomeruli and in the tubulointerstitial compartments (Figure 3ii). In comparison, the extracellular TG activity in the NTU281-treated diabetic rats remained similar to that in both normal and UNx controls throughout (Figure 3i). In agreement with less extracellular TG activity in treated animals were lower levels of catalyzed ε-(γ-glutamyl)lysine crosslinking ($P<0.05$), which were unaltered compared with the normal and UNx controls throughout the experimental period (Figure 3iii), showing continuous effective TG inhibition.

### Kidney function and albuminuria

Kidney function was assessed using serum creatinine. In untreated diabetic animals, serum creatinine rose throughout the experimental period, with more than a 3.5-fold increase by 8 months compared with that in controls (Figure 2e). Although a small increase in serum creatinine ($P<0.05$) was detected in the NTU281-treated diabetic rats by 8 months, this was 68.0% lower than that in those receiving no treatment ($P<0.05$).

Measurement of 24-h albumin excretion showed substantial increases in both treated and untreated diabetic groups by 4 months ($P<0.05$), which progressively increased at 8 months ($P<0.05$). However, in NTU281-treated animals, the increase in 24-h albumin excretion was lowered by approximately 80% at the end point (Figure 2f),

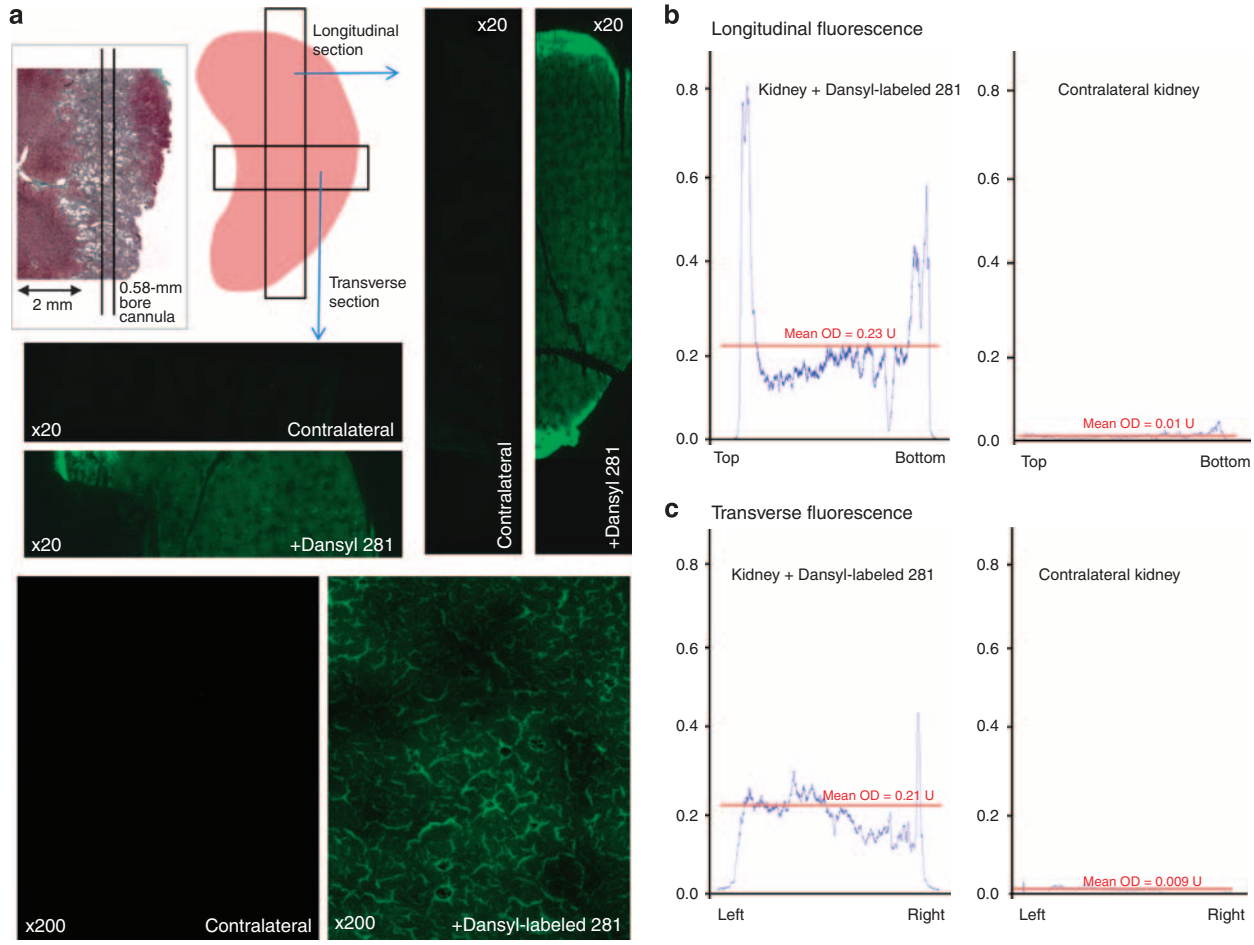


**Figure 1 | NTU281 distribution.** The kidney distribution of dansyl-labeled NTU281 (green) in both transverse and longitudinal planes from an intraparenchymal renal cannula inserted 28 days previously with 24 h drug delivery from an implanted osmotic pump (**a**). Inset shows the effect of cannulation on renal morphology on a Masson's trichrome–stained slide at 1 month. Quantification of fluorescence in comparison with the contralateral kidney in both longitudinal (**b**) and transverse (**c**) planes.

suggesting that TG inhibition slows down the deterioration of glomerular structure and function.

### Kidney scarring and morphology

After 1 month of hyperglycemia, there was no substantial difference morphologically between the four experimental groups (Figure 4a–d). By 4 months, kidney hypertrophy was well established in the UNx, treated, and untreated diabetic kidneys, with the largest increment occurring in the diabetic groups (Figure 4e–h). Furthermore, in the untreated diabetic kidney, both tubular atrophy and peritubular fibrosis were noted (Figure 4g).

No evidence of interstitial fibrosis was seen at 8 months in the normal (Figure 4i) and UNx (Figure 4j) kidneys. In comparison, in the untreated diabetic kidney (Figure 4k), there was extensive epithelial flattening, tubular atrophy, and interstitial expansion with severe tubulointerstitial scarring. Nearly all glomeruli showed advanced glomerulosclerosis, with Bowman's space filled with collagen. There was extensive expansion of the mesangial matrix, the capillary network had collapsed, and the glomeruli were extensively vacuolated. In comparison, all these changes were dramatically reduced in the NTU281-treated diabetic kidneys (Figure 4l), with only mild focal tubular epithelial flattening and a minor expansion of the tubular basement membrane.

Transmission electron microscopy of glomeruli in 8-month kidneys showed significant widespread changes in both the glomerular basement membrane (GBM) and the podocytes in untreated diabetic kidneys (Figure 5a). There was a visible thickening of the GBM and most noticeably an effacement/loss of the podocytes, especially visible at a high power (Figure 5b). Tg inhibition prevented the effacement/loss of podocytes, whereas computerized morphometric assessment of GBM thickness showed that the diabetic-induced GBM thickening was prevented with TG inhibition (Figure 5c).

### Quantification of kidney scarring

Computerized multiphase image analysis was used to assess the degree of kidney scarring on Masson's trichrome–stained sections. Assessment of glomerulosclerosis (Figure 6a) showed a significant increase in the level of fibrous tissue present by 4 months post-hyperglycemia that progressed

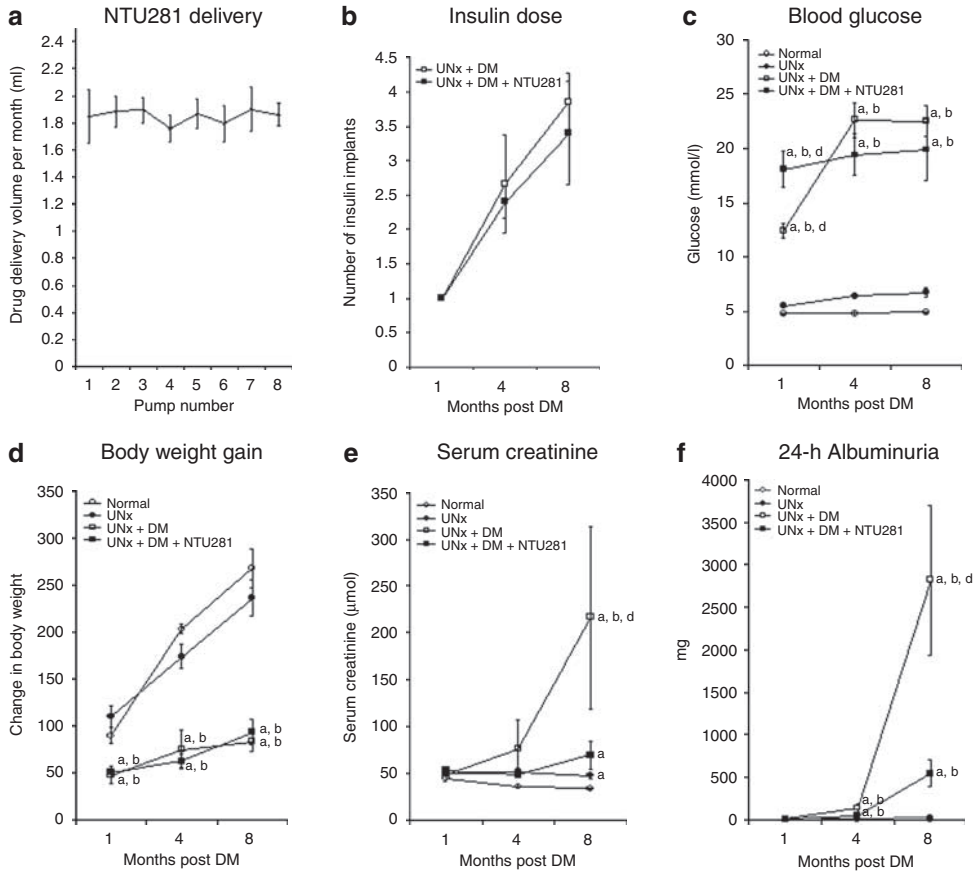


**Figure 2 | Hyperglycemia, kidney function, and drug delivery.** The volume of drug delivered per month was calculated from residual volumes in the pump (**a**). Insulin implants required to control blood glucose to 10–25 mmol/l were averaged for each experimental group (**b**). The average blood glucose of each animal over the monitoring period was determined (**c**). Changes in body weight (g) were calculated by subtracting the initial body weight from the final body weight at each time point (**d**). Kidney function was assessed by measuring serum creatinine concentration (μmol/l) (**e**). Twenty-four-hour albumin excretion (mg) was used to assess glomerular damage (**f**). White circles = normal, black circles = UNx, white squares = untreated DM, black squares = NTU281-treated DM. Data represent mean ± s.e.m., $n = 4$–7 per group. Significance ($P < 0.05$) is indicated in comparison with normal (a), UNx (b), untreated DM (c), and NTU281-treated DM (d). 'c' Indicates statistical significance compared to the untreated diabetic group.

**Table 1 | Final body weight and terminal kidney weight.**

| Time | Final body weight (g) | | | Terminal kidney weight (g) | | |
|---|---|---|---|---|---|---|
| Groups | 1 Month | 4 Months | 8 Months | 1 Month | 4 Months | 8 Months |
| Normal | 361 ± 11.7 | 472 ± 8.6 | 546 ± 22.6 | 1.0 ± 0.0 | 1.4 ± 0.13 | 1.4 ± 0.13 |
| UNx | 389 ± 7.2[a] | 447 ± 14.2 | 514 ± 15.8 | 1.4 ± 0.08[a] | 1.5 ± 0.04 | 1.7 ± 0.10 |
| UNx + DM | 319 ± 13.4[a,b] | 356 ± 20.0[a,b] | 355 ± 12.8[a,b] | 1.7 ± 0.17[a] | 3.1 ± 0.30[a,b] | 5.7 ± 0.91[a,b] |
| UNx + DM + NTU281 | 320 ± 6.7[a,b] | 350 ± 10.3[a,b] | 377 ± 14.3[a,b] | 2.3 ± 0.25[a,b,c] | 2.8 ± 0.36[a,b] | 3.3 ± 0.25[a,b,c] |

Data represent mean ± s.e.m., $n$=4–7 per group.
Significance ($P < 0.05$) is indicated in comparison with normal (a), UNx (b), and untreated DM (c).

significantly by 8 months in untreated diabetic kidneys, being fivefold that in control groups. NTU281-treated kidneys showed no significant increase in glomerulosclerosis compared with normal and UNx glomeruli over the 8-month period.

Tubulointerstitial fibrosis showed a similar trend to glomerulosclerosis, with twofold increase in scarring at 4 months rising to sixfold by 8 months in untreated diabetic animals (Figure 6b). NTU281 significantly reduced scarring in diabetic kidneys, with no detectable change compared with control at 4 months and only a twofold increase by 8 months.

### Kidney collagen content

Whole kidney collagen analysis was undertaken by measuring hydroxyproline in hydrolyzed kidney homogenates. By 8 months post-STZ, the hydroxyproline constituted 0.89 ± 0.04% of total amino acids in untreated hyperglycemic kidneys and double those in normal (0.42 ± 0.03%) and UNx

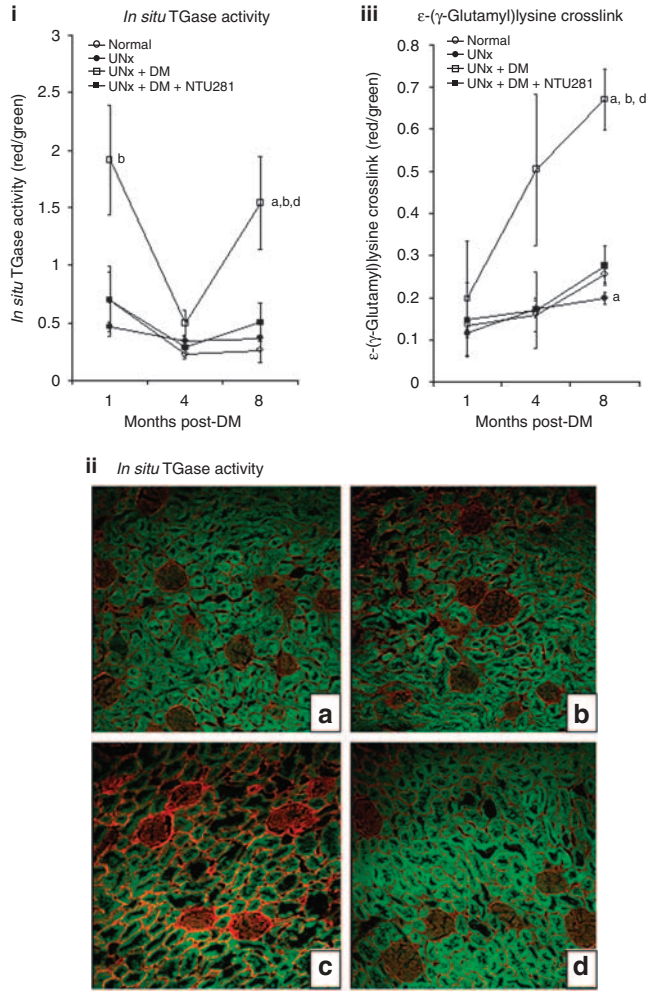


**Figure 3 | TG inhibition.** The effectiveness of NTU281 to reduce TG activity was assessed by measuring *in situ* TG activity using multiphase image analysis at 1, 4, and 8 months post-STZ (**i**). Representative TG *in situ* activity confocal microscope images at 8 months for normal (**a**), UNx (**b**), DM (**c**), and DM + NTU281 (**d**) kidneys, with TG activity shown in red (**ii**). Inhibition was confirmed by determining TG-catalyzed ε-(γ-glutamyl)lysine crosslink staining again using multiphase image analysis (**iii**). White circles = normal, black circles = UNx, white squares = untreated DM, black squares = NTU281-treated DM. Data represent mean ± s.e.m., $n = 4$–7 per group. Significance ($P < 0.05$) is indicated in comparison with normal (a), UNx (b), untreated DM (c), and NTU281-treated DM (d). STZ, streptozotocin; TG, transglutaminase. 'c' Indicates statistical significance compared to the untreated diabetic group.

animals (0.48 ± 0.03%). In NTU281-treated diabetic kidneys, hydroxyproline rose by just half that in the untreated diabetics, reaching 0.67 ± 0.03%.

Changes in collagen type I, III, and IV were investigated by immunofluorescence. In early experimental DN (1 and 4 months), there was no significant change in either collagen I (Figure 7a) or III (Figure 7b) staining in the kidney between the four experimental groups. By 8 months, both collagen I (Figure 7a) and collagen III (Figure 7b) were elevated in the untreated diabetic kidney ($P < 0.05$). Increased collagen I was mainly found in sclerotic glomeruli (Figure 8c), whereas elevated collagen III occurred in the expanded interstitium and in periglomerular areas (Figure 8g). In contrast, levels of both collagens in the NTU281-treated diabetic kidney remained similar to those in normal. Collagen IV was significantly increased by 4 months in the untreated diabetic kidney ($P < 0.05$) and continued to increase predominantly in peritubular and periglomerular areas (Figure 8k) at 8 months ($P < 0.05$). NTU281-treated diabetic kidneys had collagen IV staining levels that were comparable with the normal and UNx animals throughout experimental period (Figure 7c).

Levels of kidney scarring significantly correlated with changes in accumulation of collagen I ($r = 0.515$, $P < 0.01$), collagen III ($r = 0.718$, $P < 0.01$), and collagen IV ($r = 0.570$, $P < 0.01$).

### mRNA levels of collagen I, III, and IV

To detect if the TG inhibition had an effect on collagen synthesis, northern blotting was performed using 4- and 8-month kidneys.

At 4 months, collagen I mRNA levels in the treated diabetic kidney were similar to those in normal, but higher than those in the UNx and untreated diabetic kidneys (Figure 9a). By 8 months, collagen I mRNA levels in diabetic kidneys were significantly higher than those in the normal and UNx (Figure 9a) kidneys. The NTU281-treated kidney had levels not significantly different from those in the untreated diabetic kidney (Figure 9a).

The collagen III mRNA levels in the untreated diabetic kidney reached fivefold higher than those in the normal and UNx by 8 months (Figure 9b). In contrast, the levels in the NTU281-treated kidney were normalized at this stage, although they had been higher than those in the untreated diabetic kidney at the earlier time point (Figure 9b).

The collagen IV mRNA levels in both treated and untreated diabetic groups were similar and higher than those in the UNx group at 4 months post-STZ administration (Figure 9c). By 8 months, it was significantly increased in the untreated diabetic kidney compared with that in the other three experimental groups, with the levels more than double those in normal (Figure 9c; $P < 0.05$). Although the treated group had levels higher than those in the normal, it was not significant (Figure 9c).

Overall, the above results suggested that the TG inhibitor, NTU281, had a minimal effect on collagen I mRNA levels, but reduced the collagen III and IV mRNA levels by the end of the study.

### Myofibroblasts (α-smooth muscle actin-positive cells)

Less interstitial cells were observed on Masson's trichrome-stained sections in the TG inhibitor-treated kidney than that in the untreated. ECM-producing myofibroblasts have been reported to be associated with the progression of fibrosis in DN.[19,20] Therefore, the abundance of these cells was determined using α-smooth muscle actin (SMA) as a marker.

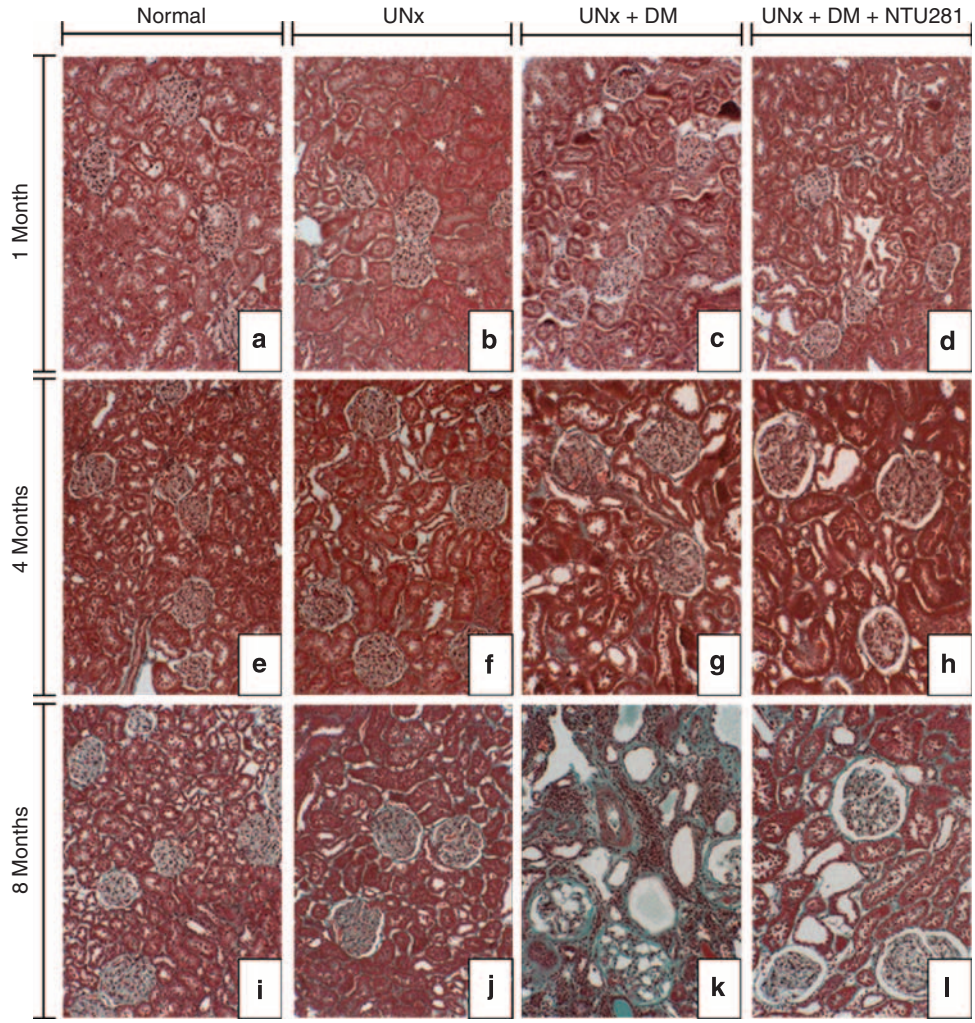


**Figure 4 | Masson's trichrome staining.** Four micrometer–thick sections from 1 month (**a**–**d**), 4 months (**e**–**h**), and 8 months (**i**–**l**) after induction of hyperglycemia were stained for Masson's trichrome (×40 magnification).

At 1 month, there were no substantial changes in α-SMA staining between any of the experimental groups, although significant increases in α-SMA staining were detected in tubulointerstitial space of both treated and untreated diabetic kidneys by 4 months (Figure 7d). This continued to increase at 8 months (Figure 7d) in the untreated group (Figure 8o). However, levels in the treated diabetic group were 67% lower than those in the untreated diabetic kidney ($P<0.05$), suggesting that TG inhibition reduced the accumulation of myofibroblasts in advanced DN.

## DISCUSSION

All current TG inhibitors block not only TG2 activity, but also other TGs such as factor XIIIa, TG1, and TG3. Hence, there is the potential for nonspecific effects that could complicate data interpretation. For example, loss of keratinocyte TG (TG1) activity has been reported to cause parakeratosis and psoriasis-like symptoms when applied to skin composites,[21,22] whereas blocking factor XIIIa may potentially lead to systemic effects such as hemorrhage and bleeding. To overcome this, we employed NTU281, an inhibitor designed to act on the outside of the cell,[23] limiting its targets to TG2 and factor XIIIa, which are the only two forms of mammalian TG known to be secreted into the extracellular space. Other potential targets such as cysteine proteases are in the main intracellular in nature, whereas concentrations up to 1 mmol/l of NTU281 do not inhibit other important cysteine-containing enzymes such as caspase-3. In addition, osmotic minipumps were employed to enable direct delivery of TG inhibitor into the kidney to minimize dose and hence systemic effects. Pressures generated by these pumps ensure that blockage is unlikely, which is supported by stable drug delivery volumes over the 8 months. Application of dansyl-labeled NTU281 showed a uniform distribution of the drug within the receiving kidney by this method. Administration of 50 mmol/l NTU281 from an implantable osmotic pump at 2.5 µl/h to the remnant kidney in the 5/6th nephrectomy (SNx) model has previously shown to halt increases in kidney TG activity without affecting blood clot stability or TG activity in other organs such as the

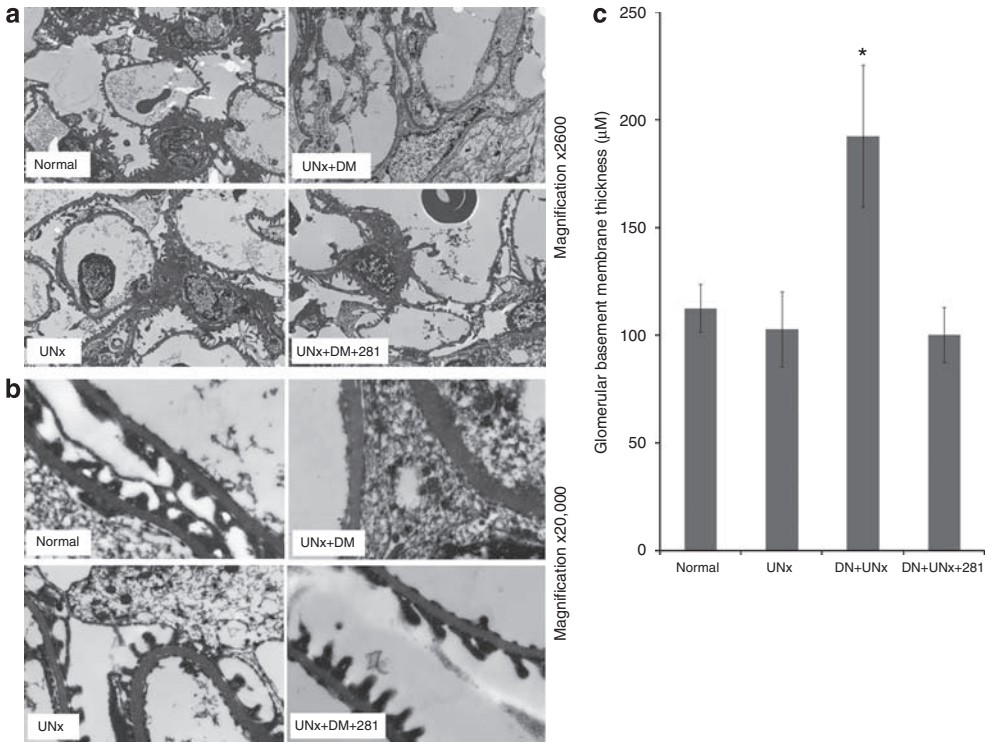


**Figure 5 | Glomerular electron microscopy.** Paraffin-embedded tissue from 8-month experimental groups was post-fixed in gluteraldehyde and observed by transmission electron microscopy at ×2600 (**a**) and ×20,000 (**b**) magnifications. Glomerular basement membrane (GBM) thickness was measured by computerized morphometric analysis by a pathologist blinded to experimental groups (**c**). Data represent mean GBM thickness ± s.e.m. *Significance from normal ($P<0.05$).

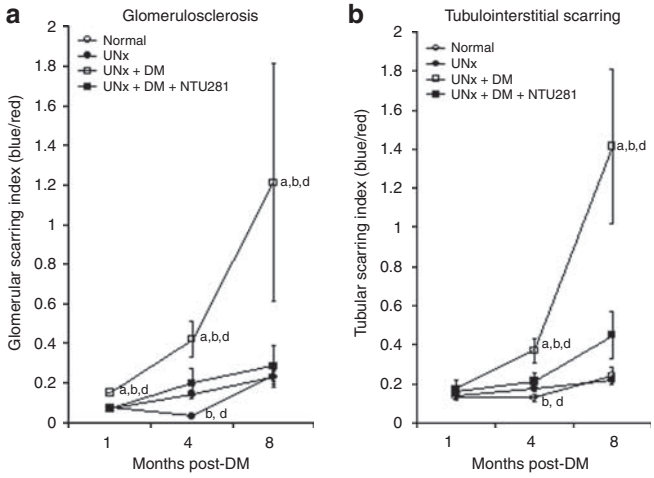


**Figure 6 | Glomerulosclerosis and tubulointerstitial scarring.** Glomerulosclerosis (**a**) and tubulointerstitial scarring (**b**) were assessed by multiphase image analysis of Masson's trichrome–stained sections. Twenty glomeruli (×400 magnification) or 10 cortical tubulointerstitial fields (×200 magnification) were analyzed per section. White circles = normal, black circles = UNx, white squares = untreated DM, black squares = NTU281-treated DM. Data represent mean ± s.e.m., $n = 4$–7 per group. Significance ($P<0.05$) is indicated in comparison with normal (a), UNx (b), untreated DM (c), and NTU281-treated DM (d). 'c' Indicates statistical significance compared to the untreated diabetic group.

heart, liver, and skin (unpublished data). Therefore, the same dose of NTU281 was used in this study and proved equally effective in reducing TG crosslinking activity in the diabetic kidney throughout the study as shown by the reduction in both TG *in situ* activity and crosslink levels, which were uniform across the treated kidney.

TG inhibition resulted in preservation of kidney function and a reduction in albuminuria as a consequence of lower levels of both glomerulosclerosis and tubulointerstitial fibrosis. On commencing this study, we expected that the underlying mechanism would be related to changes in ECM accumulation by blocking the post-translational processing of the ECM by extracellular TG, given that *in vitro* studies have repeatedly shown that TG2 alters ECM homeostasis by accelerating the rate of collagen deposition[12] and conferring the ECM with resistance to MMP proteolysis.[10] In keeping with this, we see marked reductions in mature deposited collagen I, III, and IV levels in the NTU281-treated diabetic kidneys. The levels of collagen I mRNA remained high, with levels between untreated and NTU281-treated groups identical. In contrast, levels of collagen IV mRNA were 37% lower in the treated group and those of collagen III mRNA similar to normal animals by 8 months The collagen type I mRNA data clearly support a post-transcriptional mechanism (as predicted) in the presence of a continual

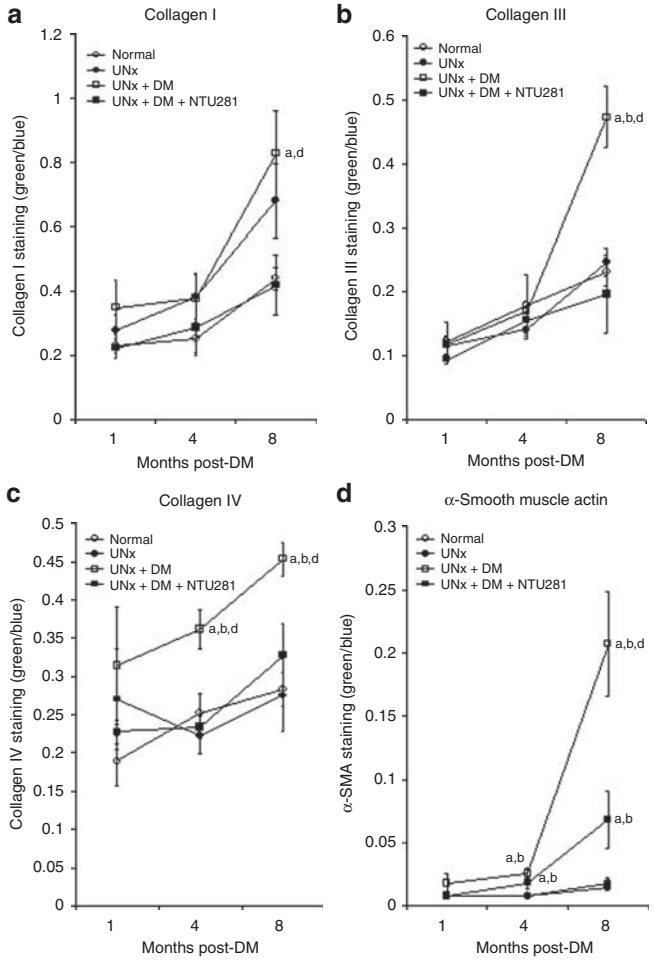


**Figure 7 | Quantification of collagen I, III, IV, and α-SMA immunostaining.** Kidney levels of collagen I (**a**), collagen III (**b**), collagen IV (**c**), and α-SMA (**d**) staining (Figure 6) were assessed by multiphase image analysis of 10 fields per section. White circles = normal, black circles = UNx, white squares = untreated DM, black squares = NTU281-treated DM. Data represent mean ± s.e.m., $n = 4$–7 per group. Significance ($P < 0.05$) is indicated in comparison with normal (a), UNx (b), untreated DM (c), and NTU281-treated DM (d). α-SMA, α-smooth muscle actin. 'c' Indicates statistical significance compared to the untreated diabetic group.

fibrotic stimuli for collagen I, but the additional, unanticipated, and interesting effect of NTU281 in suppressing type III and IV collagen mRNA levels is suggestive of an additional mechanism in lowering protein levels of these collagens.

This study was not designed to isolate particular mechanisms, and it therefore remains unclear from the data presented whether these improvements are a direct result of TG inhibition or a secondary effect caused by the reduction in fibrous tissue expansion (and thus fibrotic stimuli) brought about by lowering TGase activity. However, one could hypothesize as to two mechanisms that could lead to lower levels of collagen III and IV mRNA. It has been reported that TG2 is able to activate the fibrogenic cytokine transforming growth factor-β1 (TGF-β1) by recruiting large latent TGF-β1 in the ECM before proteolytic release of the active dimer.[24,25] Therefore, TG inhibition may affect collagen synthesis by simply altering latent TGF-β1 activation, and this may be the case for collagen III and IV although other *in vivo* (unpublished data) and *in vitro*[15] studies using TG inhibitors have failed to show lower active TGF-β1 levels. Alternatively, tubular ischemia caused by ECM expansion reducing blood flow to renal tubules may be less pronounced following NTU281 treatment. The reduction in levels of tubulointerstitial fibrosis in the treated diabetic kidney may therefore allow a better perfusion of the tubular epithelium, lowering the hypoxia-inducible factor-mediated induction of ECM proteins.[26]

Apart from the reduction in ECM accumulation, another marked effect of TG inhibition was the preservation of tubulointerstitial architecture with less tubular atrophy and interstitial myofibroblasts. Myofibroblasts undergo substantial proliferation and synthesize high levels of ECM proteins being central to the development of tubulointerstitial scarring and fibrosis.[27–29] Again, it remains unclear from our data whether these improvements are a direct result of TG inhibition or secondary to the reduction in ECM expansion.

TG inhibition was associated with a big improvement in albuminuria indicating protection of glomerular structure. Electron microscopy of glomeruli clearly showed that TG inhibition was extremely effective in the preservation of podocytes. Untreated animals had essentially no visible podocytes on the GBM, indicating either loss or pedicel retraction, whereas those receiving NTU281 had a podocyte structure and number that was not discernable from both control groups. The reason for this is most likely a combination of qualitative changes to the GBM (such as from the inclusion of collagen 1) and the 50% thicker GBM shown by morphometric measurements.

Lower levels of interstitial α-SMA-positive cells in NTU281-treated kidneys are suggestive of a reduction in myofibroblast levels, although α-SMA is not specific for myofibroblasts with smooth muscle cells in the vasculature, being particularly evident in the kidney. Epithelial–mesenchymal transdifferentiation is thought to be a major contributor to interstitial fibrosis[30,31] and thus a reduction in this could account for lower α-SMA staining. As previously mentioned, TG is known to have a role in latent TGF-β1 activation. Given TGF-β1 has been reported to be the most potent inducer of tubular epithelial–mesenchymal transdifferentiation,[32] it could be hypothesized that the increased TG activity in the diabetic kidney causes a rise in active TGF-β1 availability, resulting in the activation of myofibroblast. TG inhibition may reduce the presence of myofibroblasts by blocking TG-dependent TGF-β1-activation pathway.[10,13,33]

Of note was the variation in kidney TG activity in the untreated diabetic in this model. Both control groups and the NTU281-treated kidney showed no significant change in TG activity over the 8 months. In contrast, the DM group had a fourfold increase at 1 month, and returned to near normal at 4 months, with a threefold increase by 8 months. After

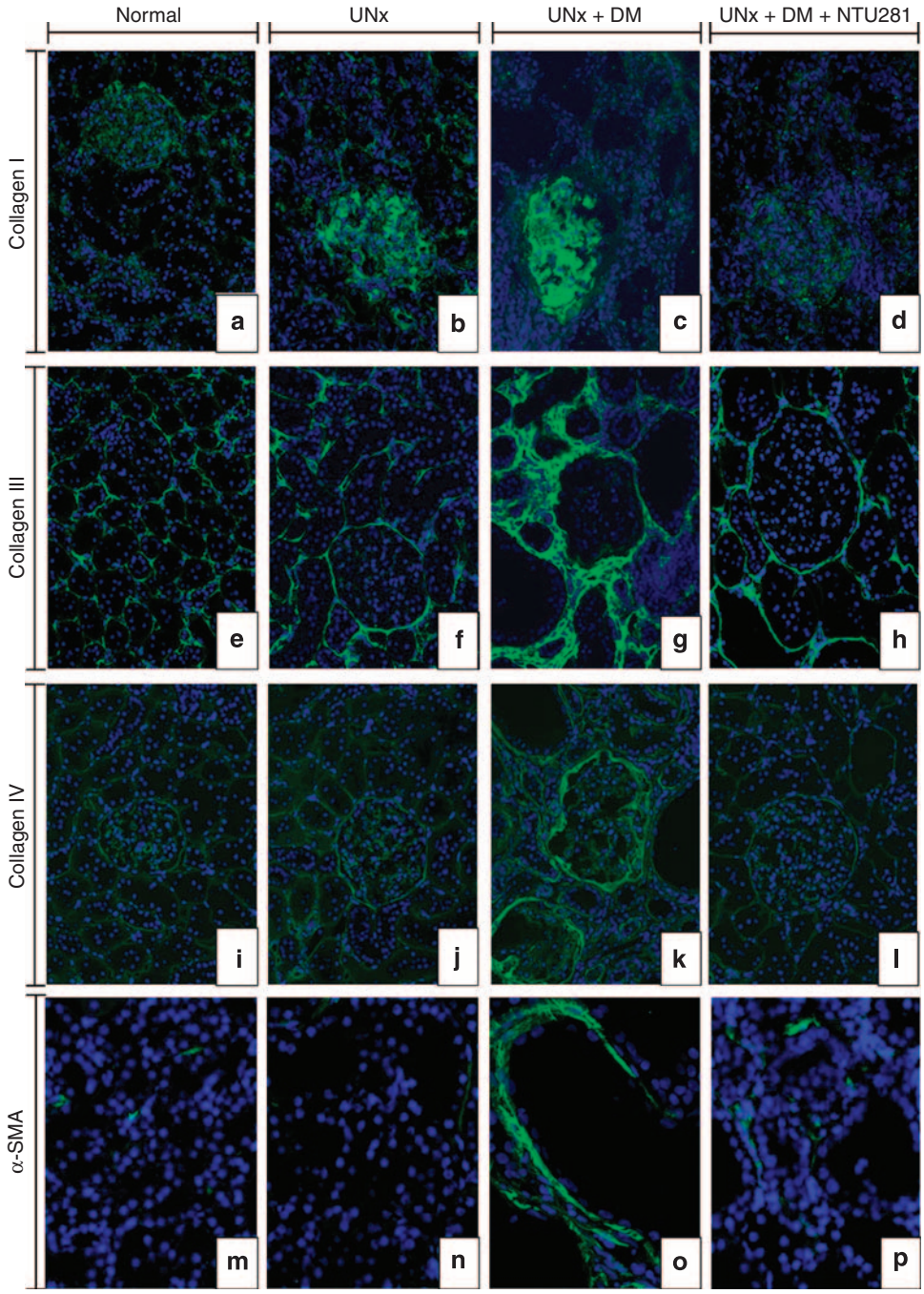


**Figure 8 | Immunofluorescent staining of collagens I, III, IV, and α-SMA in kidneys 8 months post-hyperglycemia.** Collagen I staining (**a**–**d**) was performed on cryostat sections with collagen III (**e**–**h**), collagen IV (**i**–**l**), and α-SMA (**m**–**p**) on paraffin sections. Fields were acquired at × 200 magnification on an Olympus BX61 fluorescent microscope using FITC and DAPI filter sets. DAPI, 4′,6-diamidino-2-phenylindole; FITC, fluorescein isothiocyanate; α-SMA, α-smooth muscle actin.

repeating this assay several times, we believe that this genuinely reflects the biphasic response of TG2. An early acute response to hyperglycemia, which may predominantly reflect a synthesis-independent cell export of TG2 as described previously in early DN,[13] is followed by a late remodeling response that is TG2 synthesis dependent as reported in aggressive fibrosis.[10] The discrepancy between ε-(γ-glutamyl)lysine crosslink levels and TG2 activity may seem contradictory, but is not surprising. TG2 has a half-life of around 8 h and so is quickly cleared, whereas the ε-(γ-glutamyl)lysine crosslink produced by TG2 is very stable, requiring complete digestion of the tissue to release it. Thus, if TG2 activity decreased, the crosslink would remain high.

In conclusion, TG inhibition dramatically slows the development of experimental DN through a reduction in tubulointerstitial fibrosis and glomerulosclerosis. This preserves

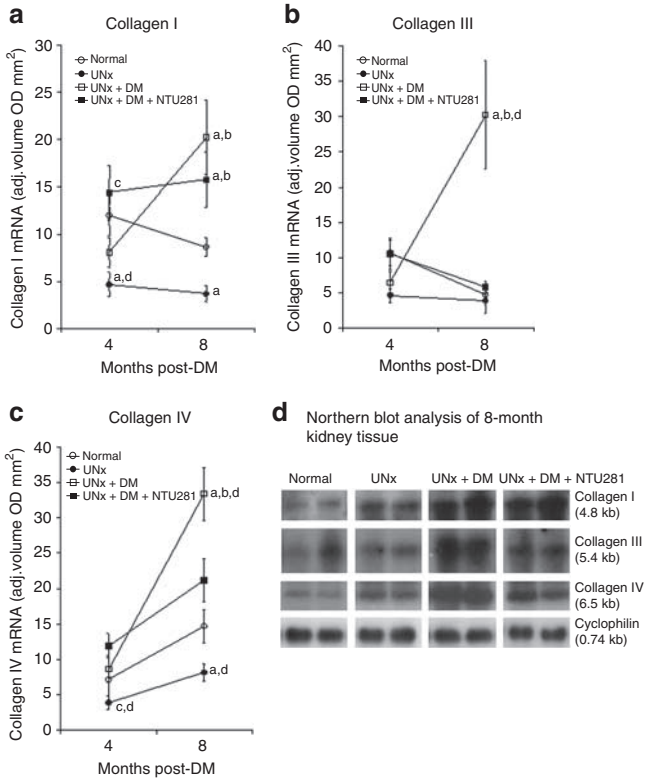


**Figure 9 | Northern blot analysis of collagen I, III, and IV mRNA.** mRNA levels of collagen I (**a**), collagen III (**b**), and collagen IV (**c**) were assessed by northern blot analysis using volume densitometry measurements normalized to the housekeeping gene cyclophilin (**d**). Some displayed autoradiographs are overexposed for diseased groups to allow clear visualization in normal kidneys. White circles = normal, black circles = UNx, white squares = untreated DM, black squares = NTU281-treated DM. Data represent mean optical density ± s.e.m., $n = 4$–7 per group. Significance ($P < 0.05$) is indicated in comparison with normal (a), UNx (b), untreated DM (c), and NTU281-treated DM (d).

kidney function and slows the development of proteinuria. The prime mechanism for this is most likely to be the lowering of the direct action of TG on ECM crosslinking that leads to matrix accumulation. The data suggest that TG inhibitors offer a potential therapeutic avenue for the amelioration of DN in the diabetic patient; however, clinical application is likely to be dependent on the development of isoform-specific compounds.

## MATERIALS AND METHODS

### Synthesis of TG inhibitor

NTU281 was synthesized according to published methods.[15] Compound purity was determined by nuclear magnetic resonance and mass spectrometry. Inhibitor efficacy was verified against renal TGs by the application of the inhibitor at 100 and 500 µmol/l to a 20% kidney homogenate, with activity measured using the [$^{14}$C] putrescine-incorporation assay.

### Experimental animals and protocol

Male Wistar Han rats (Harlan, Bicester, UK) of 200–250 g and 8–10 weeks old were subjected to right uninephrectomy (UNx). Seven days later, hyperglycemia was induced by a tail vein injection of STZ (35 mg/kg in citrate buffer, pH 4.0). Control animals were subjected to either a sham operation or UNx with vehicle injection alone. An early morning blood glucose level above 10 mmol/l at 1 week after STZ injection was considered diabetic. Blood glucose was controlled between 10 and 25 mmol/l using insulin implants (Research Pack; LinShin, Toronto, Ontario, Canada). Practically, 1/4 insulin implant was progressively inserted subcutaneously (using a trocar) until the target glucose range was reached. Measurements were taken 48 h after each 1/4 implant was inserted using a One Touch Basic glucose meter (Johnson and Johnson, Langhorne, PA, USA). Blood glucose measurements were repeated biweekly with replacement implants inserted as required.

A 0.58-mm-bore polyethylene cannula was heat sealed at one end and fenestrated between 2 and 12 mm from the seal. The open end was attached to a 2ML4 mini osmotic pump (Alzet, Cupertino, CA, USA). At UNx, the cannula was passed longitudinally through the remaining kidney such that all perforations were within the renal parenchyma. The cannula was secured using silk ties and tissue glue and run through the muscle wall to the pump located on the scruff. Pumps were loaded with either phosphate-buffered saline (vehicle) or 50 mmol/l solution of NTU281 and replaced every 28 days when exhausted.

Rats (1–4) were housed 4 to a cage at 20–22°C and 45% humidity on a 12-h light/dark cycle. They were allowed free access to standard rat chow (Labsure Ltd, Cambridge, UK) and tap water. Animals were divided into four groups: normal, uninephrectomy (UNx), diabetes with UNx (UNx + DM), and diabetes with UNx treated with NTU281 (UNx + DM + NTU281). At 1, 4, and 8 months after STZ injection, rats were killed and kidneys removed from both diabetic groups ($n \geqslant 6$) and control groups ($n = 4$). Serum creatinine was measured by standard autoanalyzer technique and 24 h albuminuria by using the Bethyl Laboratories rat albumin ELISA kit (BioGnosis, Hailsham, UK) following the manufacturer's instructions. All procedures were carried out under license according to regulations laid down by Her Majesty's Government, United Kingdom (Animals Scientific Procedures Act, 1986).

### NTU281 distribution

To ensure adequate distribution throughout the kidney, NTU281 was synthesized with a dansyl label. Animals cannulated as above were infused with phosphate-buffered saline for 1 month for the maximum fibrous coat to develop around the cannula (Figure 1a) at which stage kidneys were infused with 50 mM dansyl-NTU281 for 24 h as above. Kidneys were removed and halved longitudinally along the cannula. Cryosections were cut at 10 µm and dansyl visualized under a fluorescein isothiocyanate filter on a fluorescent microscope using the contralateral kidney as a control. Analysis 3.2 image analysis software (Soft imaging Systems, Münster, Germany) was used to generate full-length and width images using multifield alignment. These were imported into Multi Analyst (Biorad, Hemel Hempstead, UK) and a densitometric profile was generated.

### Detection of *in situ* TG activity

Cryostat sections were incubated with 0.5 mmol/l biotin cadaverine (Molecular Probes, Breda, Netherlands) and 5 mmol/l $CaCl_2$. A negative control in which $CaCl_2$ was replaced with 10 mmol/l EDTA was used. Incorporated biotin cadaverine was revealed by immunoprobing with a streptavidin indodicarbocyanine (Cy5) conjugate (Jackson ImmunoResearch, West Grove, PA, USA) at 1 in 50 dilution. Sections were visualized using a Leica TCS NT confocal microscope (Leica DMRBE; Lasertechnik, Wetzlar, Germany) using

a Kr/Ar laser (647 and 488 nm) for both Cy5 (optimal excitation 650 nm) and autofluorescence. Computer imaging was obtained at 665 and 530 nm for Cy5 and autofluorescence, respectively (Leica TCS NT; Lasertechnik). Multiphase image analysis (Analysis 3.2; Soft Imaging Systems) was performed to assess levels of incorporated cadaverine by dividing the area of red cadaverine stain with the green tissue autofluorescence to correct for tissue mass.

### Detection of ε-(γ-glutamyl)lysine crosslink

The determination of ε-(γ-glutamyl)lysine crosslink was similar to that previously described.[13] Cryostat sections were incubated with a mouse monoclonal anti-ε-(γ-glutamyl)lysine isopeptide antibody (81-D4; Covalab, Lyon, France) or mouse nonimmune serum (DAKO, Ely, UK) at 1 in 20 dilution. After washing and fixing, primary antibody was revealed using a donkey anti-mouse Cy5-conjugated antibody (Jackson ImmunoResearch). Section visualization and multiphase image analysis were performed as described above.

### Fibrosis measurement

Four-micrometer, neutral-buffered, formalin-fixed, paraffin-embedded sections were stained with Masson's trichrome (stains: collagenous material blue; nuclei, fiber, erythrocytes and elastin, red/pink). For glomerulosclerosis and tubulointerstitial scarring, 20 glomeruli ( × 400) and 10 fields ( × 200) of cortex tubules were acquired respectively in a systematic manner. A fibrous coat can develop around the renal cannula that can extend up to 1 mm in thickness (Figure 1, Masson's trichrome insert). In sections immediately above or below the cannula path, affected fields are excluded from analysis to avoid data contamination. Fibrosis was assessed using multiphase image analysis.[34] The fibrosis index was determined by dividing the area of blue collagenous stain by red cellular stain, thus correcting for cell number.

### Immunofluorescent measurements

Immunofluorescent staining was carried out on 4-μm paraffin sections using a secondary antibody conjugated with fluorescein isothiocyanate (DAKO). Following antigen retrieval, primary antibodies were applied as follows: goat anti-collagen (α1) III (1:10; Southern Biotech, Birmingham, AL, USA), rabbit anti-collagen IV (1:35; ICN, Costa Mesa, CA, USA), and mouse anti-α-SMA (1:100; DAKO). Collagen I immunofluorescence was performed on 10-μm cryostat sections using a mouse anti-collagen (α1) I antibody (1:50; Abcam, Cambridge, UK). Collagen IV antibodies were not chain specific, recognizing α1, -2, -3, and -4 chains equally.

Ten cortical fields at × 200 magnification of each section were acquired. These were analyzed using multiphase image analysis as above with correction to 4',6-diamidino-2-phenylindole staining.

### Electron microscopy

Tissue from paraffin blocks was recovered, post-fixed in gluteraldehyde, and subjected to transmission electron microscopy as previously described[35] using magnifications at × 2600 and × 20,000. GBM thickness was determined by taking at least 10 GBM measurements per glomeruli for each animal at × 20,000 magnification using Kodak AMTv600 image analysis software.

### Measurement of mRNA levels

Total RNA was extracted using TRizol (Gibco, Paisley, UK) and subjected to northern blot analysis as previously described.[36] Autoradiographs were quantified by scanning densitometry using a Biorad GS-690 densitometer and Molecular Analyst version 4 software. Densitometry values were corrected for loading using the housekeeping gene cyclophilin.[36]

### cDNA probes

Specific random primed DNA probes were constructed from the following sequences: human collagen (α1) I,[37] rat collagen (α1) III,[38] and human collagen (α1) IV.[39]

### Hydroxyproline analysis

Four hundred microliters of 10% kidney homogenates were hydrolyzed in 6 M HCl at 110°C for 18 h. These were clarified by centrifugation at 14,000 r.p.m. for 2 min and freeze-dried. This was resuspended in 400 μl of lithium loading buffer and 20 μl fractionated using a lithium chloride gradient on a Biochrom 30 amino acid analyzer as optimized by the manufacturer (Biochrom, UK). Hydroxyproline was identified against an amino-acid standard and expressed as a percentage of total amino acids.

### Statistical analysis

Data analyses were performed using one-way analysis of variance followed by a Bonferroni *post hoc* test. A probability of 95% ($P<0.05$) was taken as significant. Correlation analysis was performed on SPSS 12.0.1 for Windows.

### DISCLOSURE

The patent for compound NTU281 is held by Aston University. Professor Martin Griffin is employed by Aston University and is registered as an inventor on this patent. All the other authors declared no competing interests.

### ACKNOWLEDGMENTS

We thank the Wellcome Trust and the Sheffield Kidney Research Foundation for their financial support of this study.

### REFERENCES

1. Parving HH. Diabetic nephropathy: prevention and treatment. *Kidney Int* 2001; **60**: 2041–2055.
2. Remuzzi G, Schieppati A, Ruggenenti P. Clinical practice. Nephropathy in patients with type 2 diabetes. *N Engl J Med* 2002; **346**: 1145–1151.
3. Lameire N. Diabetes and diabetic nephropathy – a worldwide problem. *Acta Diabetol* 2004; **41**(Suppl 1): S3–S5.
4. Mosher DF. Cross-linking of fibronectin to collagenous proteins. *Mol Cell Biochem* 1984; **58**: 63–68.
5. Kleman JP, Aeschlimann D, Paulsson M *et al.* Transglutaminase-catalyzed cross-linking of fibrils of collagen V/XI in A204 rhabdomyosarcoma cells. *Biochemistry* 1995; **34**: 13768–13775.
6. Martinez J, Rich E, Barsigian C. Transglutaminase-mediated cross-linking of fibrinogen by human umbilical vein endothelial cells. *J Biol Chem* 1989; **264**: 20502–20508.
7. Kaartinen MT, Pirhonen A, Linnala-Kankkunen A *et al.* Cross-linking of osteopontin by tissue transglutaminase increases its collagen binding properties. *J Biol Chem* 1999; **274**: 1729–1735.
8. Aeschlimann D, Paulsson M. Cross-linking of laminin-nidogen complexes by tissue transglutaminase. A novel mechanism for basement membrane stabilization. *J Biol Chem* 1991; **266**: 15308–15317.
9. Fisher M, Huang L, Hau Z *et al. Over-Expression of Tissue Transglutaminase (tTg) in Proximal Tubular Epithelial (PTEC) Cells Affects ECM Accumulation In Vitro*, in Renal Association: Belfast, Northern Ireland, UK, 2005, p 246.
10. Johnson TS, Skill NJ, El Nahas AM *et al.* Transglutaminase transcription and antigen translocation in experimental renal scarring. *J Am Soc Nephrol* 1999; **10**: 2146–2157.
11. Gross SR, Balklava Z, Griffin M. Importance of tissue transglutaminase in repair of extracellular matrices and cell death of dermal fibroblasts after exposure to a solarium ultraviolet A source. *J Invest Dermatol* 2003; **121**: 412–423.

12. Fisher M, Jones RA, Huang L *et al.* Modulation of tissue transglutaminase in tubular epithelial cells alters extracellular matrix levels: a potential mechanism of tissue scarring. *Matrix Biol* 2009; **28**: 20–31.
13. Skill NJ, Griffin M, El Nahas AM *et al.* Increases in renal epsilon-(gamma-glutamyl)-lysine crosslinks result from compartment-specific changes in tissue transglutaminase in early experimental diabetic nephropathy: pathologic implications. *Lab Invest* 2001; **81**: 705–716.
14. El Nahas AM, Abo-Zenah H, Skill NJ *et al.* Elevated epsilon-(gamma-glutamyl)lysine in human diabetic nephropathy results from increased expression and cellular release of tissue transglutaminase. *Nephron Clin Pract* 2004; **97**: c108–c117.
15. Skill NJ, Johnson TS, Coutts IG *et al.* Inhibition of transglutaminase activity reduces extracellular matrix accumulation induced by high glucose levels in proximal tubular epithelial cells. *J Biol Chem* 2004; **279**: 47754–47762.
16. Fisher M, Jones R, Griffin M *et al. Primary Tubular Epithelial Cells Isolated From The Tissue Transglutaminase Knockout Mouse Deposit Less Extracellular Matrix Than Wild Type Cells*, in Renal Associate: Harrogate, UK, 2006, p 393.
17. Bower G, Brown DM, Steffes MW *et al.* Studies of the glomerular mesangium and the juxtaglomerular apparatus in the genetically diabetic mouse. *Lab Invest* 1980; **43**: 333–341.
18. Steffes MW, Buchwald H, Wigness BD *et al.* Diabetic nephropathy in the uninephrectomized dog: microscopic lesions after one year. *Kidney Int* 1982; **21**: 721–724.
19. Essawy M, Soylemezoglu O, Muchaneta-Kubara EC *et al.* Myofibroblasts and the progression of diabetic nephropathy. *Nephrol Dial Transplant* 1997; **12**: 43–50.
20. Goumenos DS, Tsamandas AC, Oldroyd S *et al.* Transforming growth factor-beta(1) and myofibroblasts: a potential pathway towards renal scarring in human glomerular disease. *Nephron* 2001; **87**: 240–248.
21. Wolf R, Lo Schiavo A, Lombardi ML *et al.* The *in vitro* effect of hydroxychloroquine on skin morphology and transglutaminase. *Int J Dermatol* 1997; **36**: 704–707.
22. Harrison CA, Gossiel F, Bullock AJ *et al.* Investigation of keratinocyte regulation of collagen I synthesis by dermal fibroblasts in a simple *in vitro* model. *Br J Dermatol* 2006; **154**: 401–410.
23. Griffin M, Mongeot A, Collighan R *et al.*: *Synthesis of potent water-soluble tissue transglutaminase inhibitors*. *Bioorg Med Chem Lett* 2008; **18**: 5559–5562.
24. Kojima S, Nara K, Rifkin DB. Requirement for transglutaminase in the activation of latent transforming growth factor-beta in bovine endothelial cells. *J Cell Biol* 1993; **121**: 439–448.
25. Nunes I, Gleizes PE, Metz CN *et al.* Latent transforming growth factor-beta binding protein domains involved in activation and transglutaminase-dependent cross-linking of latent transforming growth factor-beta. *J Cell Biol* 1997; **136**: 1151–1163.
26. Norman JT, Orphanides C, Garcia P *et al.* Hypoxia-induced changes in extracellular matrix metabolism in renal cells. *Exp Nephrol* 1999; **7**: 463–469.
27. Zeisberg M, Strutz F, Muller GA. Role of fibroblast activation in inducing interstitial fibrosis. *J Nephrol* 2000; **13**(Suppl 3): S111–S120.
28. Desmouliere A, Gabbiani G. Myofibroblast differentiation during fibrosis. *Exp Nephrol* 1995; **3**: 134–139.
29. Badid C, Mounier N, Costa AM *et al.* Role of myofibroblasts during normal tissue repair and excessive scarring: interest of their assessment in nephropathies. *Histol Histopathol* 2000; **15**: 269–280.
30. Liu Y. Epithelial to mesenchymal transition in renal fibrogenesis: pathologic significance, molecular mechanism, and therapeutic intervention. *J Am Soc Nephrol* 2004; **15**: 1–12.
31. Zeisberg M, Kalluri R. The role of epithelial-to-mesenchymal transition in renal fibrosis. *J Mol Med* 2004; **82**: 175–181.
32. Desmouliere A, Geinoz A, Gabbiani F *et al.* Transforming growth factor-beta 1 induces alpha-smooth muscle actin expression in granulation tissue myofibroblasts and in quiescent and growing cultured fibroblasts. *J Cell Biol* 1993; **122**: 103–111.
33. Johnson TS, El-Koraie AF, Skill NJ *et al.* Tissue transglutaminase and the progression of human renal scarring. *J Am Soc Nephrol* 2003; **14**: 2052–2062.
34. Johnson TS, Hau Z, Fisher M *et al. Transglutaminase Inhibition Reduce Renal Scarring by up to 92% in the Rat 5/6th Subtotal Nephrectomy (SNx) Model*, in Renal Association: Aberdeen, Scotland, UK, 2004, p 6.
35. Yang B, Johnson TS, Thomas GL *et al.* A shift in the Bax/Bcl-2 balance may activate caspase-3 and modulate apoptosis in experimental glomerulonephritis. *Kidney Int* 2002; **62**: 1301–1313.
36. Douthwaite JA, Johnson TS, Haylor JL *et al.* Effects of transforming growth factor-beta1 on renal extracellular matrix components and their regulating proteins. *J Am Soc Nephrol* 1999; **10**: 2109–2119.
37. Vuorio T, Makela JK, Kahari VM *et al.* Coordinated regulation of type I and type III collagen production and mRNA levels of pro alpha 1(I) and pro alpha 2(I) collagen in cultured morphea fibroblasts. *Arch Dermatol Res* 1987; **279**: 154–160.
38. Virolainen P, Perala M, Vuorio E *et al.* Expression of matrix genes during incorporation of cancellous bone allografts and autografts. *Clin Orthop Relat Res* 1995; **317**: 263–272.
39. Kurkinen M, Condon MR, Blumberg B *et al.* Extensive homology between the carboxyl-terminal peptides of mouse alpha 1(IV) and alpha 2(IV) collagen. *J Biol Chem* 1987; **262**: 8496–8499.